Synthesis and Biological Activity Study of Co and Cr Complexes with α-(2-Salsayl)-*N*-phenyl Nitrone and Oxide Nanoparticles

Dhamiaa Abdul-Shaheed Issa, Hayder Baqer Abdullah, and Faeza Abdulkareem Al-Mashal*

Department of Chemistry, College of Education for Pure Science, University of Basrah, 61004 Basrah, Iraq

* ***Corresponding author:***

email: faeza.nasser@uobasrah.edu.iq

Received: August 25, 2022
Accepted: January 13, 2023

DOI: 10.22146/ijc.77276

Abstract: *This paper describes the synthesis of two complexes from the ligand α-(2-Salsayl)-*N*-phenyl nitrone with $CoCl_2$ and $CrCl_2$. The ligand was characterized by several spectroscopic techniques (ultraviolet/visible (UV/Vis), nuclear magnetic resonance (^{1}H-NMR and ^{13}C-NMR), Fourier-transform infrared spectroscopy (FTIR), and mass spectrometry (MS). While infrared, ultraviolet-visible (UV-Vis), thermal analysis, and job method studies were used to reveal the structure of the complexes. The synthesized complexes were then synthesized by the sonochemical method, and the copper and chromium oxide nanoparticles were produced using the thermal decomposition method. Scanning electron microscopy (SEM), Energy dispersive X-ray spectroscopy (EDX), and X-ray diffraction (XRD) characterization confirmed the formation of Co_3O_4 and Cr_2O_3 nanoparticles. Antimicrobial studies of the complexes against some microorganisms, such as* Staphylococcus epidermis *and* Escherichia coli*, utilizing the disk diffusion method, revealed the antibacterial activity of the complexes.*

Keywords: *nitrones; complex; nanoparticles; biological activity*

■ INTRODUCTION

Nitrone is an amine that contains *N*-oxide. Nitrone derivatives preserve biological activity and are useful in pharmaceutical applications in which they are used as anti-microbial [1], electron spin spin-trapping [2-3], antioxidant [4-5], blood-brain barrier opening [6], and anti-cancer agents [7]. The nitrone group forms the electron density on the oxygen atom that assists the process of coordination bonding with metals to form a stable coordination complex [8]. Major factors affecting the coordination are the metal ion and its charge, radius, and position in the periodic table, the ligands, and the mole ratio of metal-ligand; these factors affect the stability of the complex [9-10]. Many studies have reported the formation of coordination complexes that include nitrone compounds as ligands. These ligands react with metals from transition elements, such as Zn(II), Cu(II), Ni(II), Cd(II), Co(II), and Cr(III) to form complexes that reveal high biological activity against inflammation and fungi [8,11-12]. Recently, several papers have reported exploiting compounds as capping agents for the synthesis of metal oxide nanoparticles via numerous approaches [13]. This research presents ways to control sizes and shapes using different methods, such as microwave and hydrothermal synthesis [14], thermal decomposition methods [15], and chemical precipitation [16]. The thermal decomposition of transition metal complexes is fast, practicable, economical, and solvent- and surfactant-free, resulting in precise particle size, purity, and precise process conditions [17]. This work describes the reflex and sonochemical synthesis of two new complexes of Cr(III) and Co(III) in coordination with α-(2-Salsayl)-*N*-phenyl nitrone as the ligand after which the prepared metal oxide nanoparticles were prepared using the thermal decomposition method, physical properties were studied. Furthermore, the study of the ligand and the complexes' biological activity against *Staphylococcus epidermis* and *Escherichia coli* were examined (Fig. 1).

■ EXPERIMENTAL SECTION

Materials

Reagents and solvents were obtained from Fluka or

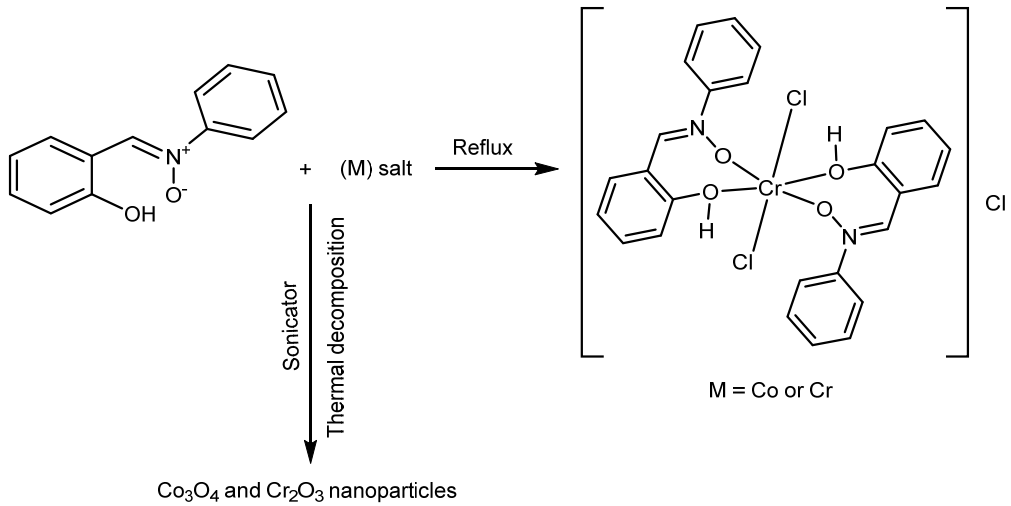

Fig 1. Schematic template of complexes and nanoparticles

Aldrich and were used as supplied. They included *N*-phenylhydroxylamine (95%), salicylaldehyde (98%), Cobalt chloride ($CoCl_2{\cdot}6H_2O$) (97%), Chromium chloride ($CrCl_2{\cdot}6H_2O$) (98%), ethanol (95%), chloroform (99%), and *n*-hexane (95%).

Instrumentation

Ultraviolet/visible (UV/Vis) spectra were characterized using PD-303 UV-Vis Spectrophotometer, and infrared (IR) spectra were recorded on a Fourier transform infrared spectrometer (FTIR-8400S, Shimadzu) at wavelengths ranging from 600 to 3800 cm^{-1}. Thermo Scientific™ FD1530M Muffle for furnace, Thermal analyses were performed using TG 209 F1 Libra. Nuclear magnetic resonance (^1H and ^{13}C-NMR) spectra were analyzed on a BRUCKER-400 MHz DMSO-d_6 solution using tetramethylsilane (TMS) as a reference. X-ray diffraction (XRD) characterization was achieved using a Philips PW 1730/10 X-Ray Diffractometer. Scanning electron microscopy (SEM) was done with a Nova NanoSEM 230.

Procedure

*Synthesis of α-(2-salsayl)-*N*-phenyl nitrone (L) [18]*

A hot solution of 0.098 g (0.09 mmol) *N*-phenylhydroxylamine in 5 mL ethanol was added to a hot solution of 0.099 g (0.09 mmol) salicylaldehyde with continuous stirring, after which the solution was refluxed for 1 h until the disappearance of reactants as verified by thin layer chromatography. The yellow crystals were recrystallized using a mixture of 3:7 ratio chloroform to *n*-hexane, and the yield was 88% with a melting point (m.p.) of 116 °C.

*Synthesis of dichlorobis(2-hydroxyphenyl)-*N*-phenylmethanimine oxide)cobalt(III) (1)*

A solution containing 0.0426 g (2.00 mmol) of **L** in 20 mL methanol was added to 0.230 g (1.00 mmol) $CoCl_2{\cdot}6H_2O$ in methanol (20 mL), after which the mixture was refluxed with a stirrer until the disappearance of reactants as verified by thin layer chromatography for 3 h. After cooling, a yellowish-green precipitate was washed with cyclohexane three times. The yield was 93%, and the m.p. was 265 °C.

*Synthesis of dichlorobis(2-hydroxyphenyl)-*N*-phenylmethanimine oxide)chromium(III) (2)*

A solution containing 0.0426 g (2.00 mmol) of **L** in 20 mL methanol was added into 0.0237 g (1.00 mmol) $CrCl_2{\cdot}6H_2O$ in methanol (20 mL), after which the mixture was refluxed with a stirrer until the disappearance of reactants as verified by thin-layer chromatography for 3 h. After cooling, the dark yellowish-green precipitate was washed with cyclohexane three times. The yield was 80%, and the m.p. of 250 °C.

Synthesis of complexes (1) and (2) via the sonochemical method

Solutions (1 L each) containing 0.170 g (0.01 mmol) in methanol (10 mL) were added to $CoCl_2{\cdot}6H_2O$ 0.090 g

(0.04 mmol) or $CrCl_2{\cdot}6H_2O$ 0.106 g (0.04 mmol). A methanol solution was added dropwise for 1 h in a 480 W (60 kHz) sonicator. The precipitate was filtered and washed with ethanol, followed by diethyl ether, dried, and saved under a vacuum desiccator.

Synthesis of metal oxide nanoparticles

Cr_2O_3 and Co_3O_4 nanoparticles were prepared via the thermal decomposition method [17]. The sonochemical method was applied to synthesize The complexes and was grounded to acquire a homogeneous powder, and afterward, the Cr(III) complex was heated at 530 °C, and the Co(III) complex was heated at 750 °C for 2 h in a muffle furnace. The resulting compound was washed with methanol 5 mL three times to remove any contamination.

■ RESULTS AND DISCUSSION

The ^{1}H-NMR spectra of **L** exhibited a singlet signal at 12.5 ppm that could be attributed to the hydroxide group proton (OH). A single signal for all spectra appeared at 8.95 ppm related to the proton of the nitrone group (-HC=NO). Moreover, the **L** exhibited multiple signals ranging from 7.9 to 6.9 ppm, ascribed to the phenyl ring's protons. Depending on integration and position, they could be explained as; 6.9 ppm related to the H^3 and H^5 due to the electron donating group (-OH), 7.5 ppm to the H^6, 7.58 ppm to the H^4, H^{10} and H^{12}, 7.6 ppm to the H^{11}, and 7.9 ppm attributed to the H^9 and H^{13}, (Fig. S1(a)).

The ^{13}C-NMR spectral data were recorded to provide additional confirmation for the ligand and exhibited a band at 146.40 ppm that was attributed to the C-OH group; in addition, a band at 159.33 ppm related to the carbon resonance of the C=NO group and another band at 117 to 137 ppm, which was attributed to the aromatic carbon resonance (Ar-C). Moreover, the spectrum shows an exceptional band for the carbon resonance of the C-NO group at 140.50 ppm (Fig. S1(b)).

The electronic spectrum of a methanol solution of **L** exhibits three bands at 335 nm (visible region) that could be ascribed to the $\pi\rightarrow\pi^*$ transitions of the nitrone group, and at 302 nm and 351 nm, the bands were ascribed to the $\pi\rightarrow\pi^*$ electronic transitions of the aromatic system. The electronic spectrum of a methanol solution of complex **1** displayed a hypsochromic shift at 349 nm and an electronic band at 532 nm that could be attributed to a *d-d* transition. Comparable results appear for complex **2**, hypsochromic shift at 325 nm for both complexes with a decrease in intensity. Moreover, complexes **2** and **3** exhibited *d-d* electronic transitions at 696 and 541 nm, respectively, verifying the coordination of the complex (Fig. S2).

IR spectra (400–4000 cm^{-1}) of **L** and complexes **1** and **2** were recorded, and a character assessment of the infrared spectra bands of the synthesized parent ligand with that of complexes is presented. The ligand exhibited significant spectra in the regions 1570, 1600, and 1174 cm^{-1} that could be ascribed to the ν(C=C), ν(C=N), and ν(N→O), respectively [19]. Moreover, a strong band at 3450 cm^{-1} was assigned to ν(O-H).

The (N→O) and ν(C=N) bands of the complexes were found to be shifted to higher values compared with that of the parent ligand, recommending the involvement of the oxygen of the nitrone group in the complex [8]. Table 1 summarizes the most important spectra of the **L** and its complexity (Fig. S3).

Thermogravimetric analysis (TGA) curves and the consistent differential thermogravimetric analysis (DTG) curves for the synthesized complex in an atmosphere of nitrogen are presented in Fig. S4. A small weight loss occurred at 56.9 °C and 98.1 °C for Cr(III) and Co(III) complexes, respectively. These peaks could

Table 1. Infrared (IR) spectra for the ligand and the complexes

Compound	Ar(C-H)	Al(C-H)	C=N	C=C	N-O	O-H
L	3082	2950	1600	1570	1174	3450
L-Co	3234	2858	1620	1601	1240	3394
L-Cr	3064	2956	1606	1571	1176	3405

be attributed to the dehydration of water adsorbed by the complexes, whereas no indication of peaks in DTG at a range around 105–145 °C, which are related to coordinated water molecules, could be found; thus, the complexes are not coordinated with water [20]. The complexes then undergo the decomposition of related ligands in two or three stages. Furthermore, the complexes show high stability reaching up to ≈800 °C, and the total weight loss and the residue for the Co(III) and Cr(III) complexes were 97.72%/3.94 mg and 97.5%/3.50 mg, respectively. The residue can be explained by considering that the weight was either metal or metal oxide, which is an indication of complex formation.

To determine the mole ratio of the ligand to the metal, the method of continuous variation method was selected. A series of solutions were prepared in which the total mole fraction amount of the metal ions and the ligand were equal for all solutions. The absorbance of the solutions was then measured against methanol as a blank. When the difference between the observed absorbance was plotted against the mole fraction of solutions, a complex containing two moles of **L** to one mole of metal for Co(III) and Cr(III) was detected.

The synthesized Co_3O_4 and Cr_2O_3 nanoparticles' crystal phases and crystallinity were studied. The XRD patterns displayed the reflection planes as exhibited in Fig. 2 and Table 3, a highly ordered cubic Co_3O_4 NPs was formed after calcination at 750 °C. This result proves the purity of phase formation and the crystal structure of the nano-metal oxide products. The annealed sample shows well-resolved Bragg peaks of the XRD pattern, which are in good correspondence with the cubic structure of the Co_3O_4 NPs. (Eq. (1)) estimated the Debye–Scherrer approximation of the average crystalline size assessment of the samples.

$$D = \frac{K\lambda}{\beta \cos\theta} \quad (1)$$

for which D represents the crystalline size, θ represents the Bragg diffraction angle, K is the Scherrer constant, λ is the wavelength (0.15406 nm), and β represents the width of the XRD peak at half maximum height. The

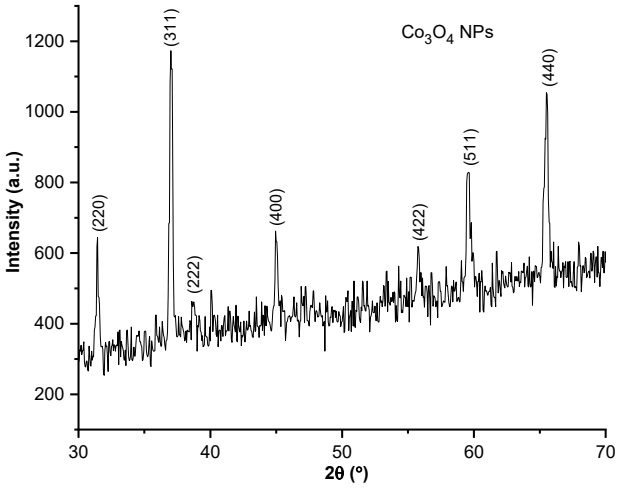

Fig 2. X-ray diffraction (XRD) patterns of the cubic Co_3O_4 nanoparticles

Table 2. The absorbance of the metal complex solutions with L using the continuous variation method

	Vm/Vt	1/10	2/10	3/10	4/10	5/10
Co(III) complex	Xvm	0.10	0.20	0.30	0.40	0.50
	ABS	0.94	0.81	0.73	0.55	0.35
Cr(III) complex	Xvm	0.1	0.2	0.3	0.4	0.5
	ABS	0.55	0.48	0.45	0.33	0.24

Table 3. X-ray diffraction analysis of Co_3O_4 nanoparticles shows estimated crystalline size for five intense peaks

Position 2θ (°)	Height (cts)	FWHM left 2θ (°)	*d*-spacing (Å)	Relative intensity (%)	Tip width	Crystalline size (D) value
31.4560	331.60	0.1968	2.84404	42.28	0.2362	41.26
37.0465	784.32	0.2460	2.42670	100.00	0.2952	35.37
44.9908	236.31	0.2952	2.01495	30.13	0.3542	27.70
59.5440	338.98	0.1968	1.55259	43.22	0.2362	41.26
65.5217	548.48	0.1968	1.42467	69.93	0.2362	41.26

Co_3O_4 NPs' average crystalline size was found to be 36.89 nm.

Fig. 3 shows the X-ray diffraction of prepared Cr_2O_3. Table 4 shows the reflection plane patterns, which imply the existence of the rhombohedral structure. In addition, no peaks could be detected due to any other material or phase, thus proving a high degree of purity of the synthesized sample after calcination at 750 °C. The broadening of the XRD lines, as seen in Fig. 3, reflects the nano-particle nature of the sample.

The sharpness of the peaks indicates good crystal growth of the oxide nanoparticles. The average particle size (D) of the particles was calculated from the intensity peaks operating the Debye–Scherrer equation, as depicted in Table 4. The calculated average crystalline size for Cr_2O_3 NPs is 30.55 nm.

Fig. 4 illustrates a scanning electron microscopy (SEM) image of prepared Co(III) and Cr(III) complexes utilizing the sonochemical method. The graph indicates a high degree of agglomeration among fine particles, mostly of nanoscale size, the diameter of the Co(III) complex was mostly between 50 and 80 nm, and the size of the Cr(III) complex was close to 112–27 nm.

Fig. 5(a) exhibits an SEM image of the Co_3O_4 NPs. The Co_3O_4 NPs crystallinity was determined, and grains of the Co_3O_4 NPs presented a closely consistent morphology with approximately 80 nm average diameter.

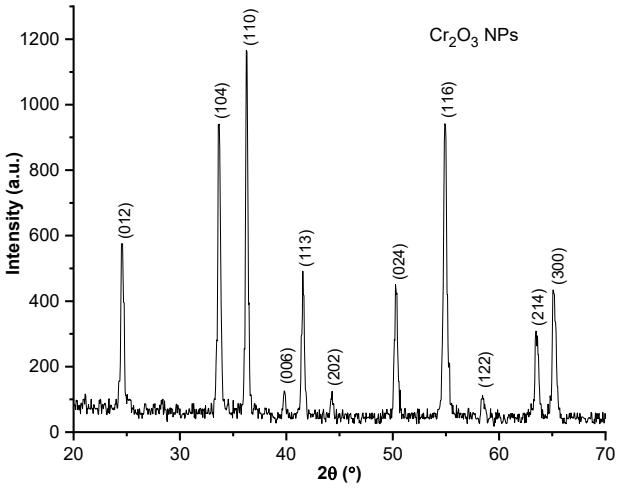

Fig 3. XRD patterns of the rhombohedral Cr_2O_3 nanoparticles

Table 4. The XRD analysis of Cr_2O_3 nanoparticles shows the estimated crystalline size for six intense peaks

Position 2θ (°)	Height (cts)	FWHM left 2θ (°)	*d*-spacing (Å)	Relative intensity (%)	Tip width	Crystalline size (D) value
24.5397	501.62	0.1968	3.62767	43.72	0.2362	41.26
33.6627	882.13	0.2952	2.66249	76.89	0.3542	27.70
36.2684	1147.27	0.2460	2.47696	100.00	0.2952	35.37
41.6022	369.99	0.2952	2.17089	32.25	0.3542	23.58
50.3359	379.96	0.3444	1.81280	33.12	0.4133	14.14
63.4590	269.07	0.1968	1.46591	23.45	0.2362	41.26

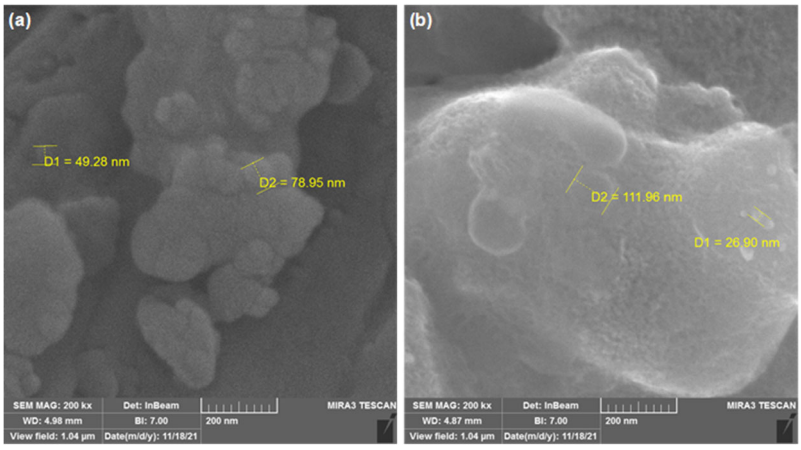

Fig 4. SEM micrograph of (a) Co(III) and (b) Cr(III) complexes prepared via the sonochemical method

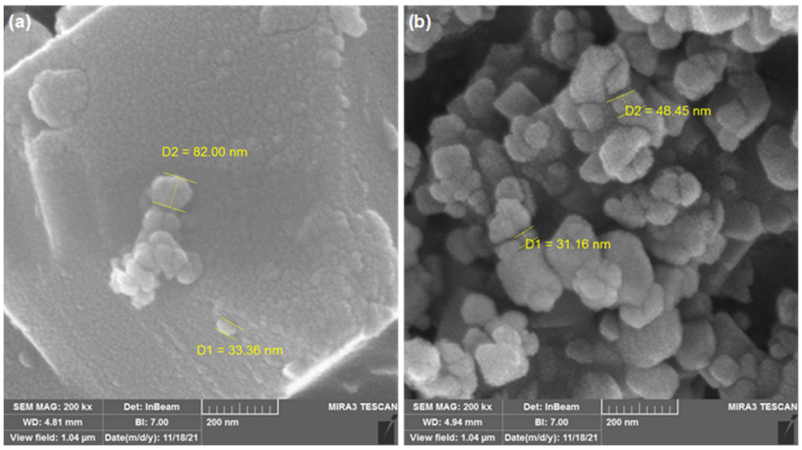

Fig 5. SEM micrograph of (a) Co_3O_4 and (b) Cr_2O_3 nanoparticles

Table 5. Antibacterial activity of different concentrations against *Escherichia coli* and *Staphylococcus epidermis*

No.	Compound	Concentration (mg/mL)	Inhibition zone (mm)	
			S. epidermis	*E. coli*
1	Ampicillin	10	29	21
2	Gentamycin	10	19	18
	L_1	50	22	18
3		25	21	12
		10	13	0
4	Co(III) CR	50	16	25
		25	15	20
		10	14	19
5	Cr(III) CR	50	25	22
		25	22	20
		10	21	18
	Co(III) NC	50	36	21
		25	24	15
		10	16	14
	Cr(III) NC	50	35	18
		25	20	18
		10	22	15

CR: complex made by reflux, NC: complex made by sonochemical

In addition, Fig. 5(b) illustrates an SEM image of the Cr_2O_3 nanoparticles. The grains of Cr_2O_3 NPs consisted of an average diameter of approximately 50 nm, indicating a uniform morphology.

The crystalline size differs from the particle size in this work since the particle characterized by XRD was a crystallized size, a crystal particle termed a primary particle, while the particles analyzed by SEM are typically particles consisting of more than primary particles.

In vitro, antibacterial activity for the Nitrone base ligand and complexes against *E. coli* and *S. epidermis* using the diffusion method were studied. This test was assessed depending on inhibition formed around the paper disks on the seeded agar plates by calculating the size basis of the zone appearing. Ampicillin and gentamycin were used as standards, Fig. S5–S10 shows the inhibition zone diameter of *E. coli and S. epidermis* by the ligand and complexes.

The results are embedded in Table 5. Evaluating the biological activity of the complex with the standard, the biological activity of the metal complexes was imminent to that of the standard. Besides, Co(III) and Cr(III) complexes synthesized by the sonochemical method affected the *E. coli* and *S. epidermis* to inhibit to the greatest degree.

■ CONCLUSION

In this paper, cobalt(III) and chromium(III) complexes from α-(2-Salsayl)-*N*-phenyl Nitrone were synthesized using the reflux and sonochemical methods and then characterized. Pure Co_3O_4 and Cr_2O_3 nanoparticles with cubic and rhombohedral structures, respectively, were well prepared via the decomposition of the complex under a muffle furnace. The thermal decomposition method is simple, practicable, and appropriate for producing high-purity products for metal oxide nanoparticles. The complexes synthesized via the two methods were selected for antibacterial activity against *E. coli* and *S. epidermis*, which are considered clinically important bacteria, and the complexes demonstrated high antibacterial activity against these types of bacteria.

■ ACKNOWLEDGMENTS

The authors gratefully acknowledge the Department of Chemistry, College of Education for Pure Sciences, University of Basrah, for the support.

■ AUTHOR CONTRIBUTIONS

Dhamiaa Abdul-Shaheed Issa conducted the experiment, Hayder Baqer Abdullah writing the original Draft and Editing, Faeza Abdulkareem Al-Mashal Supervision and revised the manuscript. All authors agreed to the final version of this manuscript.

■ REFERENCES

[1] Ferraz, M.C., Mano, R.A., Oliveira, D.H., Maia, D.S.V., Silva, W.P., Savegnago, L., Lenardão, E.J., and Jacob, R.G., 2017, Synthesis, antimicrobial, and antioxidant activities of chalcogen-containing nitrone derivatives from (*R*)-citronellal, *Medicines*, 4 (2), 39.

[2] Scott, M.J., Billiar, T.R., and Stoyanovsky, D.A., 2016, *N-tert*-butylmethanimine *N*-oxide is an efficient spin-trapping probe for EPR analysis of glutathione thiyl radical, *Sci. Rep.*, 6 (1), 38773.

[3] Pinheiro, A.C., Fazzi, R.B., Esteves, L.C., Machado, C.O., Dörr, F.A., Pinto, E., Hattori, Y., Sa, J., da Costa Ferreira, A.M., and Bastos, E.L., 2021, A bioinspired nitrone precursor to a stabilized nitroxide radical, *Free Radical Biol. Med.*, 168, 110–116.

[4] Lo Celso, F., Barone, G., Maiuolo, L., Algieri, V., Cretu, C., and Calandra, P., 2022, Dissolution of nitrones in alkylphosphates: A structural study, *J. Mol. Liq.*, 367, 120517.

[5] Chamorro, B., Diez-Iriepa, D., Merás-Sáiz, B., Chioua, M., García-Vieira, D., Iriepa, I., Hadjipavlou-Litina, D., López-Muñoz, F., Martínez-Murillo, R., Gonzàlez-Nieto, D., Fernández, I., Marco-Contelles, J., and Oset-Gasque, M.J., 2020, Synthesis, antioxidant properties and neuroprotection of α-phenyl-*tert*-butylnitrone derived *HomoBisNitrones* in *in vitro* and *in vivo* ischemia models, *Sci. Rep.*, 10 (1), 14150.

[6] Towner, R.A., Saunders, D., Lerner, M., Silasi Mansat, R., Yuan, T., Barber, D., Faakye, J., Nyul-Toth, A., Csiszar, A., Greenwood-Van Meerveld, B., and Smith, N., 2021, Temporary opening of the blood-brain barrier with the nitrone compound OKN-007, *Am. J. Nucl. Med. Mol. Imaging*, 11 (5), 363–373.

[7] Haddad, B.S., and Al-Shawi, A.A.A., 2020, Cytotoxicity of new selenoimine, selenonitrone and nitrone derivatives against human breast cancer MDA-MB231 cells, *Egypt. J. Chem.*, 63 (11), 4607–4613.

[8] Raspertova, I.V., Doroschuk, R.O., Khomenko, D.M., and Lampeka, R.D., 2017, Synthesis, spectroscopic, structural characterization of Cd(II) and Zn(II) complexes based on the *N*-methyl-C-(2-pyridyl)nitrone, *J. Coord. Chem.*, 70 (16), 2888–2899.

[9] Sorriso, S., 1982, "Structural Chemistry" in *The Chemistry of Amino, Nitroso and Nitro Compounds*

and Their Derivatives, Eds. Patai, S., John Wiley & Sons, Hoboken, New Jersey, 1–51.

[10] Hussein, K.A., and Shaalan, N., 2022, Synthesis, characterization, and antibacterial activity of lanthanide metal complexes with Schiff base ligand produced from reaction of 4,4-methylene diantipyrine with ethylenediamine, *Indones. J. Chem.*, 22 (5), 1365−1375.

[11] Thirumalaikumar, M., Sivakolunthu, S., Muthusubramanian, S., Mohan, P., and Sivasubramanian, S., 1999, Synthesis, characterization and antimicrobial studies of metal(II) bis-chelates and mixed-ligand complexes of alpha-(2-hydroxyphenyl)-*N*-(1-phenyl-2-nitroethyl)nitrone, *Boll. Chim. Farm.*, 138 (5), 207−210.

[12] Petkova, E.G., Domasevitch, K.V., Gorichko, M.V., Zub, V.Y., and Lampeka, R.D., 2001, New coordination compounds derived from nitrone ligands: Copper(II) complexes with 8-hydroxyquinoline-2-carbaldehyde- and pyridine-2-carbaldehyde-*N*-methylnitrones, *Z. Naturforsch., B: Chem. Sci.*, 56 (12), 1264−1270.

[13] Subhi, H.M., Bader, A.T., and Al-Gubury, H.Y., 2022, Synthesis and characterization of ZnO nanoparticles via thermal decomposition for Zn(II) Schiff base complex, *Indones. J. Chem.*, 22 (5), 1396−1406.

[14] Onwudiwe, D.C., 2019, Microwave-assisted synthesis of PbS nanostructures, *Heliyon*, 5 (3), e01413.

[15] Abdel-Monem, Y.K., Emam, S.M., and Okda, H.M.Y., 2017, Solid state thermal decomposition synthesis of CuO nanoparticles from coordinated pyrazolopyridine as novel precursors, *J. Mater. Sci.: Mater. Electron.*, 28 (3), 2923−2934.

[16] Bekele, B., Degefa, A., Tesgera, F., Jule, L.T., Shanmugam, R., Priyanka Dwarampudi, L., Nagaprasad, N., and Ramasamy, K., 2021, Green versus chemical precipitation methods of preparing zinc oxide nanoparticles and investigation of antimicrobial properties, *J. Nanomater.*, 2021, 9210817.

[17] Kafi-Ahmadi, L., and Shirmohammadzadeh, L., 2017, Synthesis of Co(II) and Cr(III) salicylidenic Schiff base complexes derived from thiourea as precursors for nano-sized Co_3O_4 and Cr_2O_3 and their catalytic, antibacterial properties, *J. Nanostruct. Chem.*, 7 (2), 179–190.

[18] Chen, S., Zhao, K., and Chen, G., 2015, Synthesis and application of phenyl nitrone derivatives as acidic and microbial corrosion inhibitors, *J. Chem.*, 2015, 201259.

[19] Lin-Vien, D., Colthup, N.B., Fateley, W.G., and Grasselli, J.G., 1991, "Double Bonds Containing Nitrogen Atoms" in *The Handbook of Infrared and Raman Characteristic Frequencies of Organic Molecules*, Academic Press, San Diego, 191–211.

[20] Kavitha, N., and Anantha Lakshmi, P.V., 2017, Synthesis, characterization and thermogravimetric analysis of Co(II), Ni(II), Cu(II) and Zn(II) complexes supported by ONNO tetradentate Schiff base ligand derived from hydrazino benzoxazine, *J. Saudi Chem. Soc.*, 21, S457–S466.